Journal of Alloys and Compounds 706 (2017) 16–23

Contents lists available at ScienceDirect

Journal of Alloys and Compounds

journal homepage: http://www.elsevier.com/locate/jalcom

Microstructure, mechanical properties and thermal shock resistance of ZrB_2-SiC-C_f composite with inhibited degradation of carbon fibers

Kaixuan Gui [a], Ping Hu [a, *], Wenhu Hong [b], Xinghong Zhang [a], Shun Dong [a]

[a] National Key Laboratory of Science and Technology on Advanced Composites in Special Environments, Harbin Institute of Technology, Harbin, 150001, PR China
[b] China Academy of Launch Vehicle Technology, Beijing, 100000, PR China

ARTICLE INFO

Article history:
Received 6 November 2016
Received in revised form
13 February 2017
Accepted 20 February 2017
Available online 22 February 2017

Keywords:
Ceramic composites
Fibers
Mechanical properties
Thermal shock resistance

ABSTRACT

ZrB_2-SiC-C_f composite with carbon coated carbon fibers was successfully prepared by low temperature hot pressing. This composite showed an excellent thermal shock resistance compared with those composites fabricated by hot pressing and spark plasma sintering using as-received carbon fibers. Toughening mechanisms such as crack deflection, crack branching, fibers pull-out and fibers bridging were obviously detected in ZrB_2-SiC-C_f owing to the inhibited degradation of carbon fibers and the relatively weak fiber/matrix interfacial bonding, leading to a non-brittle fracture mode of the composite. Moreover, the composite exhibited an excellent thermal shock resistance with a high critical thermal shock temperature difference of 773 °C which is about twice those of the reported ZrB_2-based ultra-high temperature ceramics. This work provides valuable guidance in the preparation of ZrB_2-based ultra-high temperature ceramics with a combination of excellent properties.

1. Introduction

ZrB_2 is typically grouped in a family of materials deemed ultra-high temperature ceramics (UHTCs) due to its high melting point (3250 °C) [1–3]. The combination of attractive properties, such as high melting temperature, high hardness and strength, high electrical and thermal conductivities and low density relative to others, makes ZrB_2 the most promising candidate for use in extreme environments [4–6]. The addition of SiC has been proved to be an effective way to improve the densification, mechanical properties as well as oxidation resistance of ZrB_2 [7,8]. Unfortunately, in spite of its distinguished properties, ZrB_2-SiC is still not capable of withstanding the extreme service environment owing to the susceptibility to brittle fracture and poor thermal shock resistance of this material [9]. In order to improve the fracture toughness and thermal shock resistance of ZrB_2-based ceramics, a verity of toughening phases have been introduced into ZrB_2 matrix, such as particles [10], graphite flakes [11], whiskers [12] and fibers [12–14]. Researches have shown that the addition of graphite (G) flakes improved the thermal shock resistance of ZrB_2-based ceramics through crack deflecting and the releasing of residual stress in the composites, while the composites still show a low fracture toughness and exhibit a typical brittle fracture mode during fracturing [15]. More recently, researchers have paid more attention to carbon fiber reinforced ZrB_2-based ceramics since the carbon fiber shows more advantages in improving the fracture toughness [14,16] and having great potential in significantly improving the thermal shock resistance of ZrB_2-based ceramics compared with other reinforcements. However, the severe degradation of carbon fibers in carbon fiber reinforced ZrB_2-based ceramics caused by the high sintering temperature has plagued researches on such materials. Therefore, it is necessary to seek ways to inhibit the degradation of carbon fibers in the fabrication of carbon fiber reinforced ZrB_2-based ceramics and the general methods should include reducing the sintering time, decreasing the sintering temperature and using carbon coated carbon fibers [16]. Spark plasma sintering (SPS) is an effective method to rapidly consolidate powders to near-theoretical density by the combined effects of rapid heating, powder surface cleaning and pressure [17], which might show advantages in reducing the sintering time of carbon fiber reinforced ZrB_2-based ceramics. The strategy typically adopted to decrease the sintering temperature of ZrB_2 is to use nanosized powders as starting material instead of micrometer powders because the sintering activity of nanosized particles is dramatically higher than that of their micrometer sized counterparts [18]. Additionally, research has

* Corresponding author.
E-mail address: huping123hit@163.com (P. Hu).

http://dx.doi.org/10.1016/j.jallcom.2017.02.227
0925-8388/

shown that deposition of carbon coating on the carbon fibers benefits to protect carbon fibers from the process corrosion during sintering [16]. However, no open literature has reported the fabrication of carbon fibers reinforce ZrB_2-based ceramics at low temperature with combination of using nanosized ZrB_2 powders and adopting carbon coated carbon fibers, and the thermal shock resistance of such material has not been investigated so far.

In this paper, as-received and carbon coated carbon fibers were adopted to fabricate ZrB_2-SiC-C_f composites using nanosized ZrB_2 powders by SPS or HP with the aim of inhibiting the degradation of carbon fibers and obtaining excellent properties of the composites. The microstructures, mechanical properties and the thermal shock behaviors of the composites were investigated.

2. Experimental procedure

Commercially available powders and carbon fibers were used in this study: ZrB_2 powders (Beijing HWRK Chem Co. Ltd., China) and SiC powders (Kaihua, China) with average particle sizes of 150 and 450 nm, respectively, and T800 carbon fibers (Tokyo, Japan) with an average diameter size of 5 μm. Prior to the fabrication process of the ZrB_2-SiC-C_f composites, continuous carbon fibers were chopped into short fibers with an average length of 2 mm. Certain amount of short carbon fibers were coated with pyrolytic carbon (PyC) using CVD process in a hot-wall tube reactor, and mixture of methane and argon gases was used to deposit PyC on the surfaces of carbon fibers at 1100 °C. The powders consisting of 50 vol% ZrB_2, 20 vol% SiC and 30 vol% carbon fibers (as-received or PyC coated) were ultrasonically dispersed in ethanol for 1 h and then ball milled for 8 h in a polyethylene bottle using WC balls and ethanol as the grinding media. To minimize segregation by sedimentation, the slurry was dried in a rotary evaporator at a temperature of 75 °C and a rotation speed of 30 rpm. The dried powders were sintered by SPS or hot pressing (HP) in a graphite die under vacuum. For SPS, the powders were heated to 1900 °C at a rate of 100 °C/min and then held at this temperature for 10 min. A uniaxial load of 30 MPa was applied at 500 °C. For HP, the powders were heated to 1600 °C at a rate of 15 °C/min and then held at this temperature for 2 h. A uniaxial load of 30 MPa was applied at 1200 °C. The shrinkage curve of the sample was recorded by a dilatometer at a resolution of 0.005 mm. The expansion of the graphite punches during sintering has a significant influence on the shrinkage curves of the powder compacts. In order to take into account the thermal expansion of punches, the entire die assembly was heated to the same temperature without the sintered powder compact inside the die. The powder shrinkage data reported in present study was obtained by subtracting the thermal expansion of the graphite punches from the original recorded shrinkage data, which could be the actual shrinkage data of the powder compact. The samples with as-received carbon fibers by SPS and HP were signed as SPS-ZSC-R and HP-ZSC-R, respectively. The sample with PyC coated carbon fibers by HP was signed as HP-ZSC-C.

Densities of ZrB_2-SiC-C_f composites were measured by the Archimedes method with deionized water as the immersing medium. Relative density was calculated via dividing bulk density by the theoretical density based on the law of mixture. Microstructures were analyzed by scanning electron microscopy (SEM, FEI Sirion, Holland) with energy dispersion spectroscopy (EDS). Flexural strength was tested in three-point bending on 3 mm × 4 mm × 36 mm bars, using a 30 mm span and a crosshead speed of 0.5 mm/min. Fracture toughness was evaluated by a single-edge notched beam (SENB) method with a 16 mm span using 2 mm × 4 mm × 22 mm test bars and a crosshead speed of 0.05 mm/min. The reported average values and standard deviations of flexural strength and fracture toughness were calculated from a minimum of six bars polished by diamond to a 0.5 μm finish. The thermal shock behaviors of the composites were investigated by a water-quenching technique. The specimens were heated to a preset temperature (200–900 °C) at a rate of 10 °C/min in a resistance furnace in air and held at this temperature for 30 min, and then the specimens were subjected to a thermal shock by quenching them into a water bath from the preset temperatures. The residual flexural strengths of the specimens after quenching were measured by three-point bending test. The reported critical thermal shock temperature difference ($\triangle Tc$) value was defined as 70% of the room temperature strength according to the linear interpolation of the residual strength values as described in ASTM C1525-04 [19].

3. Results and discussion

Fig. 1 displayed the typical fracture surfaces of SPS-ZCS-R prepared by SPS at 1900 °C for 10 min. It can be clearly seen that serious degradation of carbon fibers occurred in the composite during the SPS process. Most of the carbon fibers were transformed into carbon clusters as shown in Fig. 1a. A small portion of carbon fibers seemed to survive in the composite while they were also severely destroyed during the SPS process as indicated in Fig. 1b and c. ZrC was obviously detected by EDS on the surfaces of the carbon fibers, as shown in inset of Fig. 1b, indicating that some reactions occurred between carbon fibers and other compositions containing zirconium element. According to the results of thermodynamic calculation, the change in Gibbs free energy of the reaction between carbon and ZrB_2 was positive at the present condition, which demonstrated that the carbon fiber should not react with ZrB_2. In general, surface oxidation of commercially available ZrB_2 and SiC powders, especially for nanosized powders, was inevitable to be hindered during production or reserve, and the equimolar amounts of ZrO_2 and B_2O_3 impurities could be formed on the surfaces of ZrB_2 powders due to the oxidation of the powders under ambient conditions [20]. The reaction between carbon and ZrO_2 impurity were thermodynamically favorable at the present condition, which should be the main reason for the formation of ZrC phase causing the degradation of carbon fibers. In addition, the reactions between carbon fibers and B_2O_3 and SiO_2 impurities existed on the surfaces of the ZrB_2 and SiC powders, respectively, should be also responsible for the serious degradation of carbon fibers. From the microstructure analysis of ZrB_2-SiC-C_f composite by SPS, it can be concluded that the degradation of carbon fibers could not be inhibited by reducing the sintering time at high temperature (1900 °C).

In order to reduce the sintering temperature and achieve an acceptable level of density, ZrB_2-SiC-C_f composite with as-received carbon fibers was hot pressed at 1600 °C with a holding time of 2 h. As expected, most of the carbon fibers in HP-ZSC-R preserved their integrity during the hot pressing process compared with those in SPS-ZCS-R shown in Fig. 2, although a much longer sintering time was used to densify HP-ZSC-R. Comparing with the different microstructure evolutions of carbon fibers in SPS-ZCS-R and HP-ZSC-R, it can be concluded that the high sintering temperature was the main factor leading to the degradation of carbon fibers and reducing the sintering temperature was an effective way to inhibit fiber degradation. Even so, surface erosion of carbon fibers was inevitable in HP-ZSC-R (Fig. 2c) because of the reactions between carbon fibers and other compositions. In order to further understand the surface erosion mechanisms of carbon fibers, the element distribution near the fiber/matrix interface was investigated by EDS as exhibited in Fig. 3. It can be clearly seen that the amounts of oxygen and silicon located at the fiber/matrix interface were significantly higher than those located in the matrix and carbon fibers implying a segregation of SiO_2 at the fiber/matrix interface.

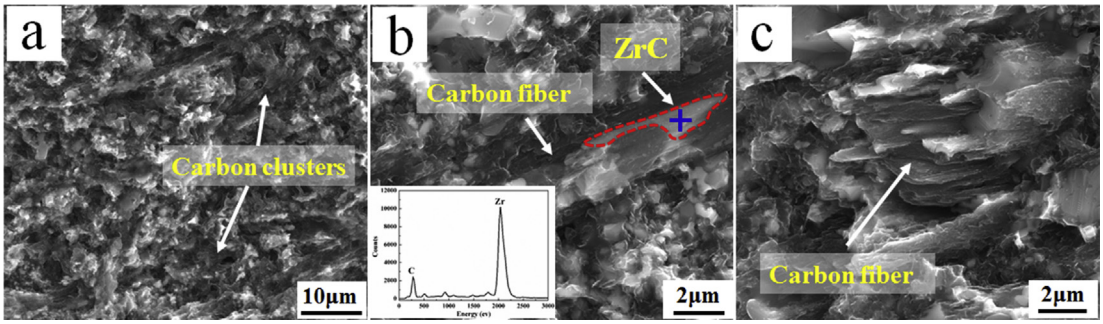

Fig. 1. Microstructures of SPS-ZCS-R prepared by SPS at 1900 °C for 10 min.

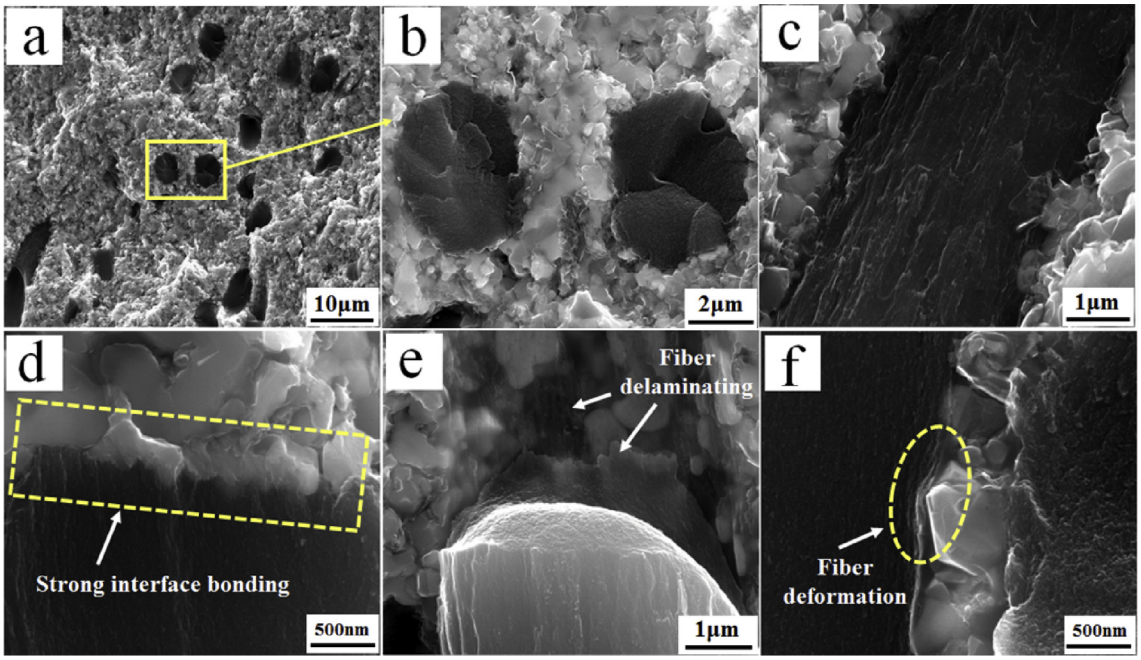

Fig. 2. Microstructures of HP-ZSC-R fabricated by hot pressing at 1600 °C for 1 h.

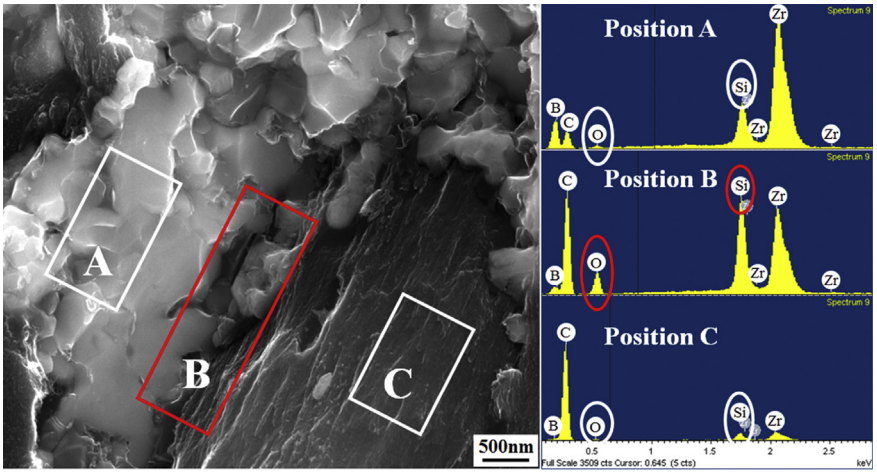

Fig. 3. EDS patterns of element distribution near the fiber/matrix interface of HP-ZSC-R.

Similar research had shown that SiO_2 liquid phase had the tendency to move towards ZrB_2/C_f interface by capillary forces that attracted the liquid in the areas with voids between fiber and ZrB_2 [21]. The segregation of SiO_2 at the fiber/matrix interface would

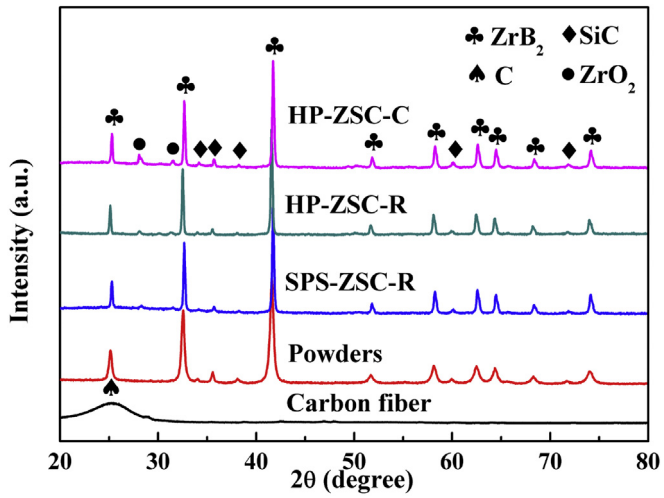

Fig. 4. XRD patterns of as-received carbon fiber, mixed ZrB_2-SiC-C_f powders and sintered composite.

facilitate the reaction between carbon fiber and SiO_2, which might be the main reason for the surface erosion of the carbon fibers in HP-ZSC-R. It should be noted that almost no carbon fibers pulled out from the fracture surface of HP-ZSC-R shown in Fig. 2a and b. An extensive fiber pull-out indicates a relatively weak fiber/matrix interfacial bonding, while a flat fracture surface indicates a strong fiber/matrix interfacial bonding [22]. From Fig. 2d, HP-ZSC-R exhibited a strong fiber/matrix interfacial bonding that even resulted in the fiber delaminating (Fig. 2e). Therefore, the flat fracture surface of HP-ZSC-R should be attributed to the strong fiber/matrix interfacial bonding. In addition to chemical reaction that could lead to a strong fiber/matrix interfacial bonding, physical bite strength could also increase the fiber pullout-resistance. Fig. 2f revealed a typical fiber deformation caused by the physical bite between carbon fiber and ZrB_2 grain.

In order to further inhibit the degradation of carbon fibers and weaken the fiber/matrix interfacial bonding, PyC coated carbon fibers were used to fabricate ZrB_2-SiC-C_f composite by hot pressing at 1600 °C for 2 h. The XRD patterns of as-received carbon fibers, mixed ZrB_2-SiC-C_f powders and hot-pressed composites were plotted in Fig. 4. Only ZrB_2 and SiC peaks were detected in the mixed powders, while no carbon peaks were observed indicating that the adopted carbon fibers might have a poor degree of graphitization, which was certified by XRD pattern of carbon fiber. Meanwhile, the disappearance of the diffusion peak of carbon fiber could also be ascribed to similar diffusion angles of carbon fiber and the (0001) peak of ZrB_2. Weak m-ZrO_2 peaks were detected in XRD patterns of SPS-ZSC-R, HP-ZSC-R and HP-ZSC-C that could not be found in the raw powders, which might be attributed to the crystallization of ZrO_2 impurity present on the ZrB_2 powders during hot pressing. In addition, the peak width of ZrB_2 in the mixed powders was clearly larger than that of hot-pressed ZrB_2-SiC-C_f composite as a result of the grain growth during sintering.

The microstructure of PyC coated carbon fibers was shown in Fig. 5. It can be clearly seen that most of the as-received carbon fibers were coated by a PyC layer (detected by EDS) with a thickness of about 5 μm. No obvious structure evolution occurred in the carbon fibers during the CVD process implying that the process individually did not caused the degradation of carbon fibers. The SEM images of the fracture surface for HP-ZSC-C were shown in Fig. 6. Both the internal and surface structures of the carbon fibers in HP-ZSC-C were well preserved after sintering indicating that the degradation of carbon fibers was effectively inhibited with the help of coating and decreasing sintering temperature. Moreover, HP-ZSC-C displayed extensive fibers pull-out as compared with HP-ZSC-R, as shown in Fig. 6a and b, which should be attributed to both the weak fiber/matrix interfacial bonding and the inhibited degradation of carbon fibers. Research had shown that the PyC interfacial layer is a low interfacial shear strength and easy slipping interfacial layer, a huge amount of interface debonding and cracks deflection and branching would occur in the interface but the efficiency of the load transfer through the interfacial layer would reduce [16], which would weaken the interfacial adhesion between carbon fibers and matrix. The weak fiber/matrix interfacial bonding provided a relative low interfacial shear stress and the inhibited degradation of carbon fibers allowed fibers to have sufficient strength withstanding the interfacial shear stress. It should be noted that some PyC layers disappeared from the surfaces of the carbon fibers in HP-ZSC-C after mechanical testing, which should be ascribed to the fact that the carbon fibers pulled out from the PyC coatings as shown in Fig. 6d. The thickness of some PyC coatings seemed to be less than 5 μm, which might be attributed to the compacting force in the PyC layer caused by the applied pressure during hot pressing.

Fig. 7 showed the images of crack propagation path on the surface of HP-ZSC-C after SENB test. Some toughening effects associated with carbon fibers were clearly observed in HP-ZSC-C, such as crack deflection, crack branching, fibers pull-out and fibers bridging. Firstly, when a propagating crack encountered a carbon fiber, it would propagate along the fiber/ceramic interface because the interface had a weaker bonding strength as compared with carbon fiber, resulting in the crack deflection shown in Fig. 7b.

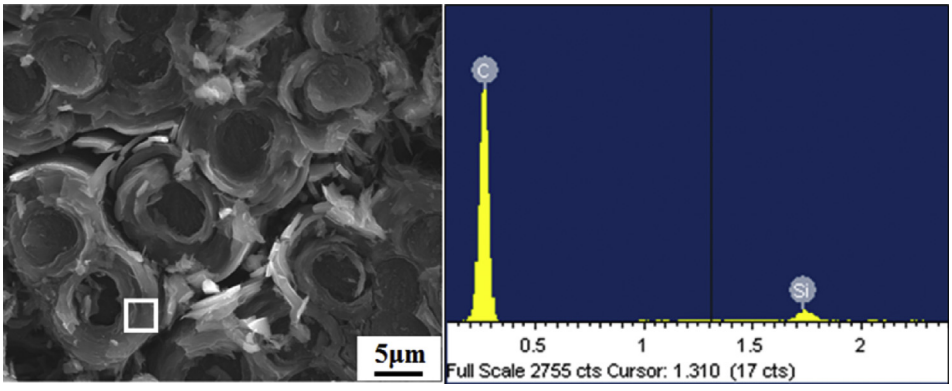

Fig. 5. SEM image of carbon coated carbon fibers used in the present study and the EDS pattern of the coating.

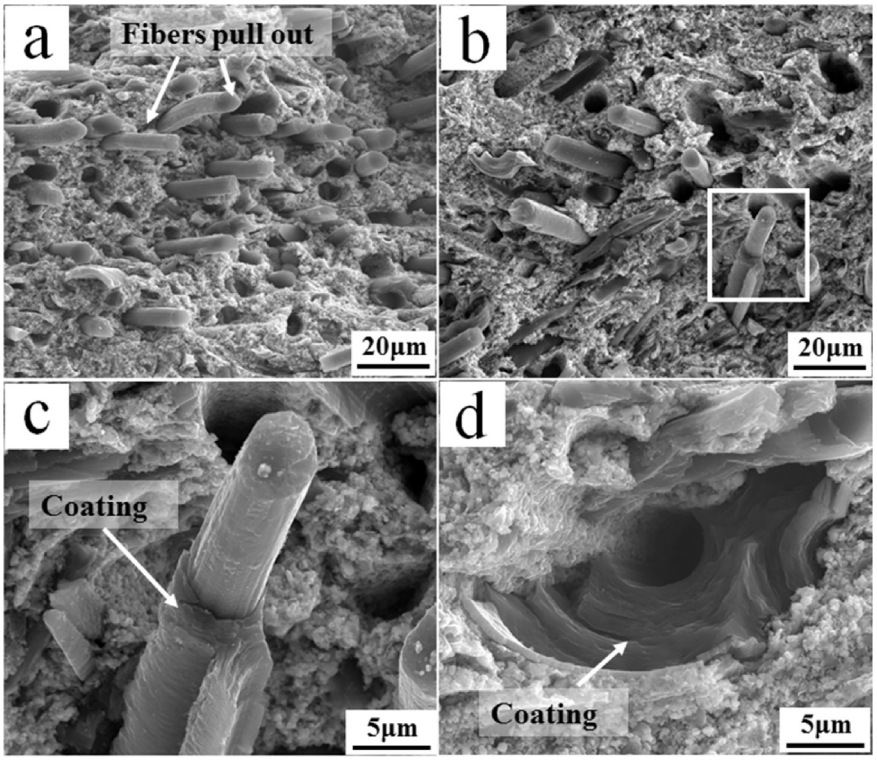

Fig. 6. Microstructures of HP-ZSC-C consolidated by hot pressing at 1600 °C for 2 h.

On the other hand, the deflection of the main crack was generally accompanied by the generation of micro-cracks (Fig. 7c), i.e. crack branching, leading to the energy-dissipation of the main crack. In addition, fibers pull-out and fibers bridging were also detected on the surface of HP-ZSC-C. It is believed that these mechanisms, especially for crack deflection, can extend the crack path and absorb crack-propagating energy [23].

The relative densities and mechanical properties of ZrB_2-SiC-C_f

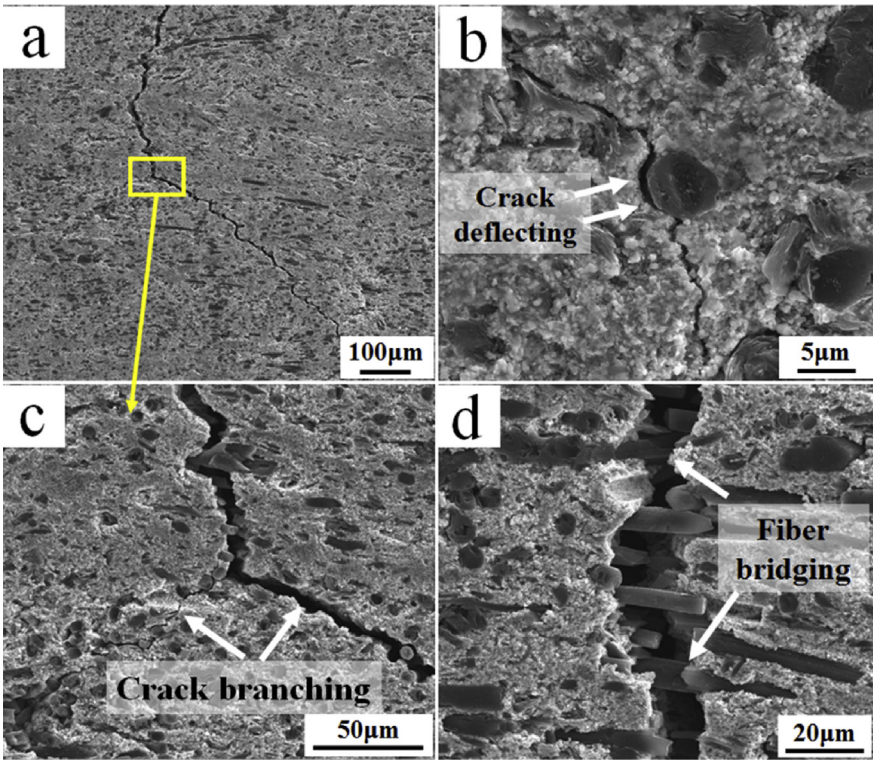

Fig. 7. Typical crack propagation path on the surface of HP-ZSC-C after SENB test.

Table 1
Relative densities and mechanical properties of ZrB_2-SiC-C_f composites fabricated by different processes.

Sample	Sintering process	Relative density (%)	Flexural strength (MPa)	Fracture toughness (MPa $m^{1/2}$)
SPS-ZSC-R	SPS, 1900 °C, 10 min	98.7	345 ± 54	3.21 ± 0.12
HP-ZSC-R	HP, 1600 °C, 120 min	95.8	335 ± 17	4.56 ± 0.13
HP-ZSC-C	HP, 1600 °C, 120 min	95.3	317 ± 12	6.16 ± 0.15

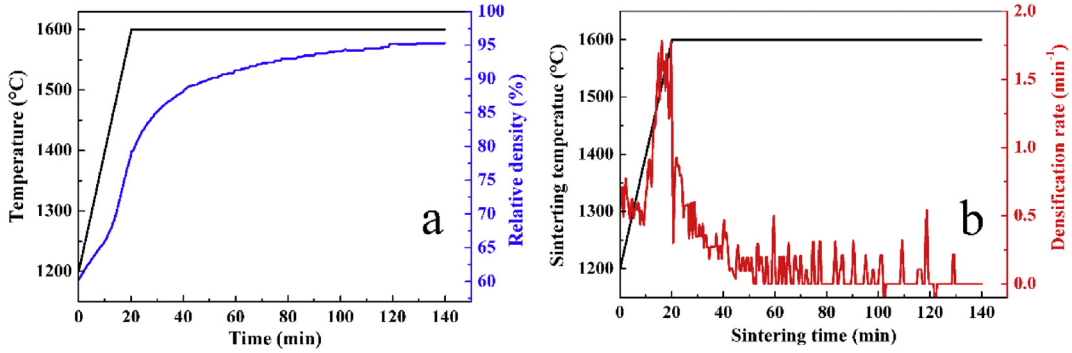

Fig. 8. Densification (a) and densification rate (b) versus sintering time curves of HP-ZSC-C.

composites fabricated by different processes were shown in Table 1. SPS-ZSC-R had a relative density of 98.8% which was higher than those of HP-ZSC-R and HP-ZSC-C due to the high sintering temperature and the SPS technique which was reported to be an effective method to enhance the densification of ZrB_2-based ceramics [24]. Although the investigated composites had comparable flexural strengths, HP-ZSC-R and HP-ZSC-C had significantly lower standard deviation values of the flexural strength as compared with SPS-ZSC-R demonstrating that the inhibition of fibers degradation in ZrB_2-SiC-C_f composites could improve their mechanical property stabilities. It is noted that HP-ZSC-C with low interfacial adhesion still possessed comparable flexural strengths as the HP-ZSC-R, which might be ascribed to inhibited degradation of carbon fibers in HP-ZSC-C. Due to the serious degradation of carbon fibers in SPS-ZSC-R, the toughening mechanisms were hindered leading to a low fracture toughness of the composite (3.21 ± 0.12 MPa $m^{1/2}$) which is comparable to the monolithic ZrB_2 [25]. In spite of having the similar relative densities and flexural strengths, HP-ZSC-C had a much higher fracture toughness (6.16 ± 0.15 MPa $m^{1/2}$) than that of HP-ZSC-R (4.56 ± 0.13 MPa $m^{1/2}$). The improved fracture toughness for HP-ZSC-C should be ascribed to the effectively inhibited fibers degradation and the weak fiber/matrix bonding that allowed the operation of toughening mechanisms such as fibers pull-out, fibers bridging, crack branching and crack deflection as discussed above.

In order to investigate the densification behavior of ZrB_2-SiC-C_f composite with PyC coated carbon fibers, the relative density and densification rate versus sintering time curves of sample HP-ZSC-C were traced as soon as the applied pressure stabled at 30 MPa (corresponding temperature 1200 °C), shown in Fig. 8. From Fig. 8a, it can be seen that the densification of HP-ZSC-C had started at 1200 °C with a densification rate of about 0.5 min^{-1}. In general, the onset sintering temperature of microsized ZrB_2 powders was observed at ~1700 °C [26], much higher than the present value, confirming that the nanosized ZrB_2 powders significantly reduced the sintering temperature of ZrB_2-SiC-C_f composite. From Fig. 8b, rapid densification occurred at the temperature range of 1400–1600 °C and a maximum densification rate of 1.78 min^{-1} was achieved at 1520 °C, while it decreased gradually at the holding stage until the densification was ceased. The final relative density achieved 95.3% for HP-ZSC-C which was a considerable value with the consideration of the low sintering temperature (1600 °C), which should be attributed to the high sintering activity of the nanosized ZrB_2 powders.

Typical load-displacement curves of three different ZrB_2-SiC-C_f composites during SENB test were given in Fig. 9 to investigate the fracture behaviors of the composites. As shown in Fig. 9, the curves of SPS-ZSC-R and HP-ZSC-R displayed linear behaviors up to failure loads and then the crack rapidly propagated resulting in catastrophic failures of the composites. In other words, SPS-ZSC-R and HP-ZSC-R showed typical brittle fracture modes. Whereas, in case of HP-ZSC-C, the curve showed a small load drop after the first crack followed by an increase in load again to the maximum value, and then the load gradually decreased resulting in the tailed shape of the load-displacement curve. Namely, HP-ZSC-C exhibited a non-brittle fracture mode. The noticeable difference in the fracture behaviors of these composites should be accounted by the microstructure of carbon fibers as well as the fiber/matrix bonding strength in the composites. The serious degradation or surface erosion of carbon fibers combined with the strong fiber/matrix bonding strength were the main reasons for the brittle fractures of SPS-ZSC-R and HP-ZSC-R. The effectively inhibited degradation of carbon fibers and relatively weak fiber/matrix bonding strength offered substantial toughening for HP-ZSC-C and led to the non-brittle fracture of the composite. In addition, the elastic modulus of the composite (the slope of the flexural stress-strain curve before fracture) decreased from SPS-ZSC-R to HP-ZSC-R to HP-ZSC-C, and the decrease in elastic modulus was believed to be beneficial to improve the thermal shock resistance of the ZrB_2-based ceramics [27].

The thermal shock behaviors of ZrB_2-SiC-C_f composites prepared by different processes were investigated by water-quenching method, and the residual flexural strengths versus thermal shock temperature differences for the composites were shown in Fig. 10. The residual strength of SPS-ZSC-R varied little when the temperature difference was lower than 400 °C while it decreased sharply to 52% of the initial strength when quenched at 500 °C, resulting in a critical temperature difference of 463 °C. In contrast, the residual strength of HP-ZSC-R after thermal shock was statistically equivalent to the original strength as the thermal shock temperature difference increased up to 600 °C and it decreased gradually with

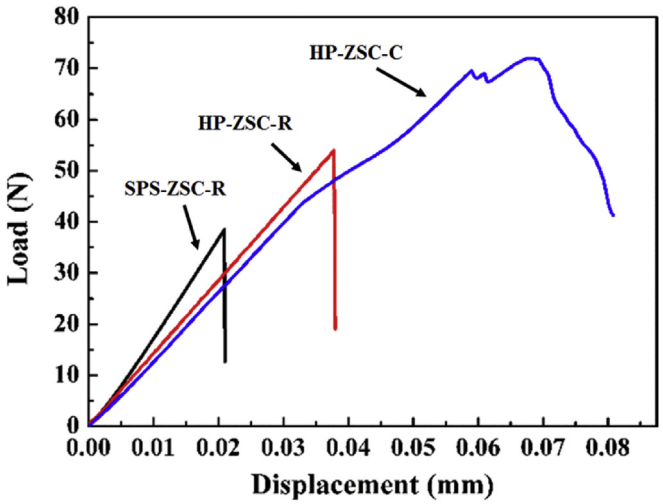

Fig. 9. Typical load-displacement curves of ZrB_2-SiC-C_f composites by different processes during SENB test.

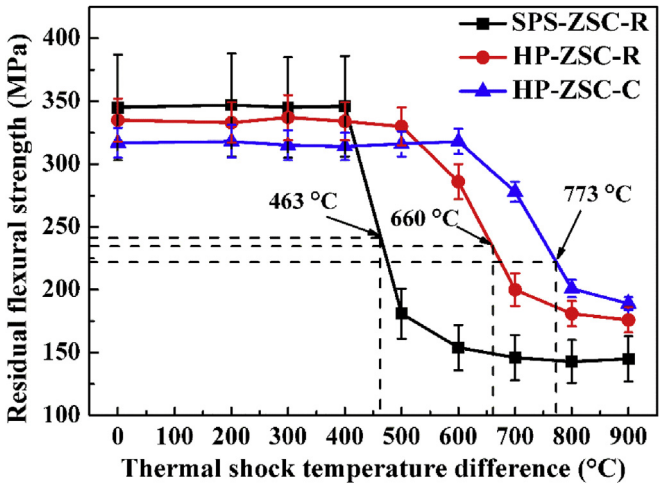

Fig. 10. Residual flexural strength versus thermal shock temperature difference for ZrB_2-SiC-C_f composites by different processes.

the further increased thermal shock temperature difference. The measured critical thermal shock temperature difference was 660 °C for HP-ZSC-R, dramatically higher than that of SPS-ZSC-R. In case of HP-ZSC-C, the residual strength almost kept stable as the thermal shock temperature difference was increased up to 700 °C and then gradually decreased as the thermal shock temperature difference increased. A high thermal shock temperature difference of 773 °C was achieved for HP-ZSC-C, almost twice those of the reported ZrB_2-based UHTCs. The enhanced thermal shock resistance of HP-ZSC-C was mainly attributed to the improvement in fracture toughness and the reduction in flexural strength according to the fracture criterion [28]:

$$\alpha_{cr} = K_{IC}^2/(\pi\sigma^2)$$

where α_{cr} is critical crack size, σ is the flexural strength and K_{IC} is the fracture toughness. The fracture of brittle ceramic results from the propagation of inherent flaws with sizes beyond the critical crack size leading to the catastrophic failure of the ceramic [28], which implies that a larger critical crack size results in a higher damage tolerance. The calculated critical crack size for HP-ZSC-C was 120.3 μm, much higher than those of SPS-ZSC-R (27.6 μm) and HP-ZSC-R (59.0 μm), which should be responsible to the high thermal shock temperature difference of the HP-ZSC-C. The present study confirmed that the combination of reducing the sintering temperature using nanosized ZrB_2 powders and introduction of carbon coated carbon fibers was an effective way to inhibit the degradation of carbon fibers in ZrB_2-SiC-C_f composites, which can significantly improve the thermal shock resistance of such materials.

4. Conclusions

ZrB_2-SiC-C_f composites were fabricated by SPS and HP using naonsized ZrB_2 powders, and the microstructure evolutions of carbon fibers in the composites were investigated. SPS of ZrB_2-SiC-C_f at high temperature with a short holding time caused a serious degradation of carbon fibers resulting in a poor fracture toughness and a brittle fracture mode of the composite. Although the degradation of carbon fibers was well suppressed in ZrB_2-SiC-C_f by HP at low temperature, the surface erosion and the strong fiber/matrix interface bonding hindered the fibers pull-out leading to a brittle fracture. The degradation of carbon fibers was effectively inhibited in HP ZrB_2-SiC-C_f owing to the low sintering temperature and the addition of carbon coated carbon fibers instead of as-received carbon fibers. As a result, the composite showed a typical non-brittle fracture mode which should be attributed to toughening mechanisms such as fibers pull-out, fibers bridging, crack branching and crack deflection. Furthermore, a high critical thermal shock temperature difference of 773 °C was achieved for ZrB_2-SiC-C_f composite with carbon coated carbon fibers, almost twice those of the reported ZrB_2-based UHTCs, confirming an excellent thermal shock resistance of the composite. This study provides great guidance in the preparation of ZrB_2-based UHTCs with a combination of excellent properties.

Acknowledgements

Financial support was provided by the National Nature Science Foundation of China (Project Nos. 51272056, 11121061, 51372047 and 91216301), the National Fund for Distinguished Young Scholars (No. 51525201) and the Fundamental Research Funds for the Central Universities (Grant No. HIT.BRETIII.201506).

References

[1] L.Y. Xiang, L.F. Cheng, L. Shi, X.W. Yin, L.T. Zhang, Mechanical and ablation properties of laminated ZrB_2-SiC/BN ceramics, J. Alloys Compd. 638 (2015) 261–266.
[2] G. Gautam, A. Mohan, Effect of ZrB_2 particles on the microstructure and mechanical properties of hybrid (ZrB_2+Al_3Zr)/AA5052 insitu composites, J. Alloys Compd. 649 (2015) 174–183.
[3] Y. Wang, J. Liang, W.B. Han, X.H. Zhang, Mechanical properties and thermal shock behavior of hot-pressed ZrB_2-SiC-AlN composites, J. Alloys Compd. 475 (1) (2009) 762–765.
[4] S.Q. Guo, Densification of ZrB_2-based composites and their mechanical and physical properties: a review, J. Eur. Ceram. Soc. 29 (6) (2009) 995–1011.
[5] W.B. Han, G. Li, X.H. Zhang, J.C. Han, Effect of AlN as sintering aid on hot-pressed ZrB_2-SiC ceramic composite, J. Alloys Compd. 471 (1) (2009) 488–491.
[6] A. Chamberlain, W. Fahrenholtz, G. Hilmas, Low-temperature densification of zirconium diboride ceramics by reactive hot pressing, J. Am. Ceram. Soc. 89 (12) (2006) 3638–3645.
[7] W. Guo, G. Zhang, Oxidation resistance and strength retention of ZrB_2-SiC ceramics, J. Eur. Ceram. Soc. 30 (11) (2010) 2387–2395.
[8] W.C. Tripp, H.H. Davis, H.C. Graham, Effect of a SiC addition on the oxidation of ZrB_2, Ceram. Bull. 52 (8) (1973) 612–616.
[9] Z. Wang, S. Wang, X.H. Zhang, P. Hu, W.B. Han, C.Q. Hong, Effect of graphite flake on microstructure as well as mechanical properties and thermal shock resistance of ZrB_2-SiC matrix ultrahigh temperature ceramics, J. Alloys Compd. 484 (1) (2009) 390–394.
[10] F. Monteverde, Beneficial effects of an ultra-fine α-SiC incorporation on the sinterability and mechanical properties of ZrB_2, Appl. Phys. A 82 (2) (2006)

329–337.
[11] Z. Wang, Z.J. Wu, G.D. Shi, Fabrication, mechanical properties and thermal shock resistance of a ZrB_2-graphite ceramic, Int. J. Refract. Met. Hard Mater 29 (3) (2011) 351–355.
[12] L. Silvestroni, D. Sciti, C. Melandri, S. Guicciardi, Toughened ZrB_2-based ceramics through SiC whisker or SiC chopped fiber additions, J. Eur. Ceram. Soc. 30 (11) (2010) 2155–2164.
[13] J. Lin, X.H. Zhang, Z. Wang, W.B. Han, Microstructure and mechanical properties of ZrB_2-SiC-ZrO_{2f} ceramic, Scr. Mater 64 (9) (2011) 872–875.
[14] F.Y. Yang, X.H. Zhang, J.C. Han, S.Y. Du, Mechanical properties of short carbon fiber reinforced ZrB_2-SiC ceramic matrix composites, Mater. Lett. 62 (17) (2008) 2925–2927.
[15] Y. Hou, P. Hu, X.H. Zhang, K.X. Gui, Effects of graphite flake diameter on mechanical properties and thermal shock behavior of ZrB_2-nanoSiC-graphite ceramics, Int. J. Refract. Met. Hard Mater 41 (2013) 133–137.
[16] K.S. Xiao, Q.G. Guo, Z.J. Liu, S. Zhao, Y. Zhao, Influence of fiber coating thickness on microstructure and mechanical properties of carbon fiber-reinforced zirconium diboride based composites, Ceram. Int. 40 (1) (2014) 1539–1544.
[17] G.D. Zhan, J.D. Kuntz, J. Wan, A.K. Mukherjee, Single-wall carbon nanotubes as attractive toughening agents in alumina-based nanocomposites, Nat. Mater 2 (1) (2003) 38–42.
[18] V. Zamora, A. Ortiz, F. Guiberteau, M. Nygren, Crystal-size dependence of the spark-plasma-sintering kinetics of ZrB_2 ultra-high-temperature ceramics, J. Eur. Ceram. Soc. 32 (2) (2012) 271–276.
[19] J.W. Zimmermann, G.E. Hilmas, W.G. Fahrenholtz, Thermal shock resistance of ZrB_2 and ZrB_2-30% SiC, Mater. Chem. Phys. 112 (1) (2008) 140–145.
[20] M. Thompson, W. Fahrenholtz, G. Hilmas, Effect of starting particle size and oxygen content on densification of ZrB_2, J. Am. Ceram. Soc. 94 (2) (2011) 429–435.
[21] L. Silvestroni, D. Dalle Fabbriche, C. Melandri, D. Sciti, Relationships between carbon fiber type and interfacial domain in ZrB_2-based ceramics, J. Eur. Ceram. Soc. 36 (1) (2016) 17–24.
[22] X.L. He, Y.K. Guo, Y. Zhou, D.C. Jia, Microstructures of short-carbon-fiber-reinforced SiC composites prepared by hot-pressing, Mater. Charact. 59 (12) (2008) 1771–1775.
[23] K.T. Fabert, A.G. Evans, Crack deflection processes-I. theory, Acta Metall. 31 (4) (1983) 565–576.
[24] S.Q. Guo, T. Nishimura, Y. Kagawa, J.M. Yang, Spark plasma sintering of zirconium diborides, J. Am. Ceram. Soc. 91 (9) (2008) 2848–2855.
[25] A.L. Chamberlain, W.G. Fahrenholtz, G.E. Hilmas, D.T. Ellerby, High-strength zirconium diboride-based ceramics, J. Am. Ceram. Soc. 87 (6) (2004) 1170–1172.
[26] M. Thompson, W.G. Fahrenholtz, G. Hilmas, Effect of starting particle size and oxygen content on densification of ZrB_2, J. Am. Ceram. Soc. 94 (2) (2011) 429–435.
[27] M. Aldridge, J.A. Yeomans, The thermal shock behaviour of ductile particle toughened alumina composites, J. Eur. Ceram. Soc. 19 (9) (1999) 1769–1775.
[28] D. Taylor, P. Cornetti, N. Pugno, The fracture mechanics of finite crack extension, Eng. Fract, Mech 72 (7) (2005) 1021–1038.